A Generalized Energy Balance Climate Model with Parameterized Dynamics and Diabatic Heating

KAREN M. SHELL* AND RICHARD C. J. SOMERVILLE

Scripps Institution of Oceanography, University of California, San Diego, La Jolla, California

(Manuscript received 18 March 2004, in final form 13 August 2004)

ABSTRACT

Energy balance models have proven useful in understanding mechanisms and feedbacks in the climate system. An original global energy balance model is presented here. The model is solved numerically for equilibrium climate states defined by zonal average temperature as a function of latitude for both a surface and an atmospheric layer. The effects of radiative, latent, and sensible heating are parameterized. The model includes a variable lapse rate and parameterizations of the major dynamical mechanisms responsible for meridional heat transport: the Hadley cell, midlatitude baroclinic eddies, and ocean circulation. The model reproduces both the mean variation of temperature with latitude and the global average heat budget within the uncertainty of observations.

The utility of the model is demonstrated through examination of various climate feedbacks. One important feedback is the effect of the lapse rate on climate. When the planet warms as a result of an increase in the solar constant, the lapse rate acts as a negative feedback, effectively enhancing the longwave emission efficiency of the atmosphere. The lapse rate is also responsible for an increase in global average temperature when the meridional heat transport effectiveness is increased. The water vapor feedback enhances temperature changes, while the latent and sensible heating feedback reduces surface temperature changes.

1. Introduction

Climate models range in complexity from simple, one-equation analytic models to state-of-the-art earth system computer models, simulating the physics, chemistry, and biology of the earth's surface, atmosphere, cryosphere, and oceans. Although the goal, understanding the climate, is the same, the specific strengths and weaknesses, and thus appropriate uses, of climate models can be quite different.

Much recent work has focused on improving complex models such as oceanic, atmospheric, and coupled general circulation models (GCMs). To make explicit predictions (e.g., temperature change associated with anthropogenic climate forcing), the level of detail provided by GCMs is necessary. However, GCMs lack (by design) the clarity that makes simple models, such as energy balance (North et al. 1981) and radiative convective models, useful. A simple model provides a conceptual picture of the processes, without the complicating details of a GCM (assuming, of course, one wisely chooses "processes" to include and "details" to omit). A GCM, on the other hand, includes so many potential feedback processes that it is often difficult to unravel cause and effect or isolate a single feedback process. In addition, natural variability within a complex model may overwhelm a small but realistic climate signal. Finally, the computational requirements of GCMs prevent a thorough exploration of parameter space. A broad range of parameterizations can be studied with a simple model, providing a more comprehensive understanding of possible system behavior.

Thus, a range of model complexity is useful. Simple models can provide conceptual understanding of the climate system, which can then be tested in more complex models. Complex models often provide a more realistic, but harder to interpret, result. Both types of models, as well as a spectrum of models of intermediate complexity (Claussen et al. 2002), will be useful in developing a comprehensive understanding of the climate system.

* Current affiliation: National Center for Atmospheric Research, Boulder, Colorado.

Corresponding author address: Dr. Karen M. Shell, National Center for Atmospheric Research, 1850 Table Mesa Drive, Boulder, CO 80305.
E-mail: kshell@ucar.edu

Our model may be thought of as a new type of zonal-average energy balance model (EBM) related to those first developed by Budyko (1969) and Sellers (1969). EBMs describe the climate system in terms of thermodynamics (i.e., temperature). Dynamical variables, such as wind speed, are not treated explicitly. Our model differs from traditional EBMs in two important ways. First, the model includes a simple vertical structure. It treats the surface and the atmosphere separately and thus uses two temperatures rather than one to describe the system at each latitude. It also utilizes a prognostic lapse rate to represent vertical structure within the atmosphere. Second, the model includes parameterizations of the effects of dynamical processes, such as the Hadley circulation and midlatitude eddies, on the temperature and lapse rate. These model properties allow us to explore feedbacks not normally considered in EBMs.

EBMs are designed to study the climate sensitivity to an imposed radiative forcing, such as a change in the amount of incoming solar radiation or the concentration of greenhouse gases. The climate response depends not only on the direct heating or cooling caused by the radiation change, but also on feedbacks within the system, which amplify or damp the temperature change. There are many possible feedbacks within the climate system; a complete model must correctly include all the important feedbacks in order to accurately predict climate change. EBMs can be used to determine the sign and approximate magnitude of various feedbacks. The results suggest which feedbacks are significant and deserving of further study in GCMs.

EBMs traditionally lack vertical resolution, using a single temperature for the entire column. Thus, some feedbacks related to the vertical profile of temperature are lacking. We focus on three particular feedbacks not typically explored in EBMs: the water vapor/emissivity feedback, the latent and sensible heat flux feedback, and the lapse rate feedback. The emissivity feedback is thought to be one of the dominant atmospheric feedbacks and has been often studied in radiative–convective models (Manabe and Wetherald 1967), which have the multiple layers generally required to resolve it. The lapse rate feedback has also been explored only in true multilayer models (Wetherald and Manabe 1975). Finally, the latent and sensible heat flux feedback can only be studied in models with a separate surface and atmospheric layer [a simple version of this is included in Held and Suarez (1974), though not seriously explored]. We have developed a model that allows study of these vertically related feedbacks such that we can resolve them while retaining as simple a model as possible.

These feedbacks are sometimes implicitly included in EBMs. For example, the standard $A + BT$ outgoing longwave radiation parameterization (Budyko 1969) is based on observations and thus automatically includes feedbacks related to water vapor and lapse rate changes, as well as the net effect of latent and sensible heat flux changes, on the top-of-atmosphere (TOA) outgoing longwave radiation. With this parameterization, however, it is impossible to isolate the individual feedbacks. Our model, on the other hand, allows the processes to operate independently for easier exploration of their behavior alone and in combination with other feedbacks. In this paper, we demonstrate the utility of our model by studying the effects of these processes on climate sensitivity to changes in the solar constant.

The model's vertical "pseudo" resolution also allows more detailed parameterizations of meridional heat transport. Atmospheric heat transport is calculated separately from ocean transport. In this paper, we begin an exploration of the climate response to changes in the atmospheric or oceanic heat transport, focusing on the interactions between the heat transport efficiency and the emissivity, lapse rate, and latent and sensible heat feedbacks in the model.

2. Model description

The model consists of a longitudinally averaged atmospheric layer above a surface layer, which represents the combined influences of ocean and land. The only spatial coordinate is latitude, which is resolved by a grid from pole to pole. The temperatures of the atmosphere (T_a) and surface (T_s) are determined for each latitude (ϕ) as a function of time (t) by the sum of several heating and cooling mechanisms:

$$C_a \frac{\partial T_a}{\partial t} = S_a + I_a + F_s + F_l + D_a, \tag{1}$$

$$C_s \frac{\partial T_s}{\partial t} = S_s + I_s - F_s - F_l + D_s, \tag{2}$$

where C is the heat capacity, S is the net solar (shortwave) heating, I is the net infrared (longwave) heating, F_s and F_l are the sensible and latent heat fluxes from the surface to the atmosphere, and D is the rearrangement of heat due to dynamical effects. The subscripts a and s refer to atmospheric and surface values, respectively. We are interested in steady-state solutions, such that the temperatures are constant in time, and the right-hand-side terms cancel. Computationally, we step Eqs. (1) and (2) forward in time using the forward difference scheme from a specified initial state (usually an

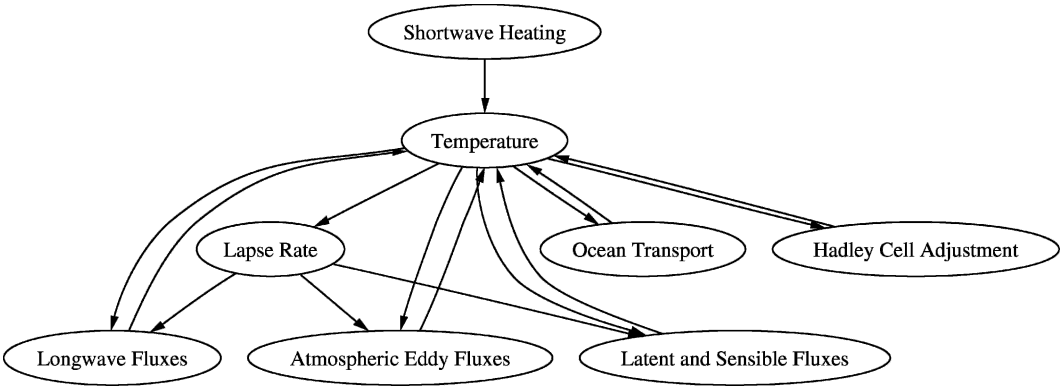

FIG. 1. Model components. Arrows indicate the direction of influence.

isothermal state or a previous steady state) until the sum of the magnitudes of atmospheric and surface temperature changes per time step is less than a specified value, δ, multiplied by the time step, Δt.

Each heating term is parameterized in terms of the atmospheric and surface temperature, as described in the following section. Figure 1 illustrates the interactions among the main components of the model.

a. Lapse rate and boundary layer temperature

Our model includes a simple parameterization of atmospheric vertical structure using a prognostic average atmospheric lapse rate that varies as a function of latitude. In middle and high latitudes, the lapse rate is set to the critical lapse rate for baroclinic adjustment:

$$\mathrm{lr} = \Gamma + \frac{\tan\phi}{H_l}\frac{\partial T_a}{\partial \phi}, \tag{3}$$

from Stone (1978). Here Γ is the dry-adiabatic lapse rate, and H_l is the scale height, which is treated as a free parameter and tuned to produce the observed lapse rate. The critical lapse rate is the theoretical lapse rate when baroclinic perturbations become unstable and thus efficient at transporting heat. Observations suggest that long-term averages of middle- and high-latitude lapse rates are close to this critical lapse rate (Stone 1978).

In the Tropics, we use the equatorial lapse rate, assuming a boundary layer relative humidity, r. We integrate the temperature with height starting from the boundary layer temperature, T_{bl}, described below. The temperature increases at the dry-adiabatic lapse rate until the air is saturated; then it increases at the moist-adiabatic lapse rate. We use the temperature difference between the boundary layer and 10 km to determine the average lapse rate. This atmospheric lapse rate is used throughout the Tropics since tropical temperatures vary little with latitude. The lapse rate transitions from the tropical lapse rate to the baroclinic lapse rate at the latitude where the two are equal.

Using the lapse rate, we calculate the boundary layer temperature,

$$T_{\mathrm{bl}} = T_a + \mathrm{lr} \times H_m, \tag{4}$$

where H_m is the representative height of the atmospheric layer, a specified constant.

b. Solar radiation

The solar radiation parameterization uses the fractional reflectivity (R), absorptivity (A), and transmissivity (T) of the atmosphere to incident light, such that $A + R + T = 1$; R, T, and A depend on the direction of the light (either from above or below the layer). Variables with asterisks (i.e., R^*, A^*, and T^*) correspond to the atmosphere's effect on light from below, while variables without asterisks correspond to light from above. The surface albedo (α_s) and incoming solar radiation (S) are also used in the calculation.

Figure 2 shows the possible pathways for solar radiation and calculates the amount of solar radiation following each path, using the adding method (Liou 2002). Incoming solar radiation is reflected to space, absorbed, or transmitted by the atmosphere. Solar radiation that reaches the ground is either absorbed or reflected. The reflected radiation is absorbed by the atmosphere, lost to space, or reflected back to the ground. Multiple reflections between the atmosphere and ground are included.

From Fig. 2, the top-of-the-atmosphere (TOA) shortwave heating (incident solar radiation less reflected) is

$$S_{\mathrm{TOA}} = S\left(1 - R - \frac{TT^*\alpha_s}{1 - \alpha_s R^*}\right). \tag{5}$$

The shortwave surface heating (net solar radiation absorbed by the surface) is

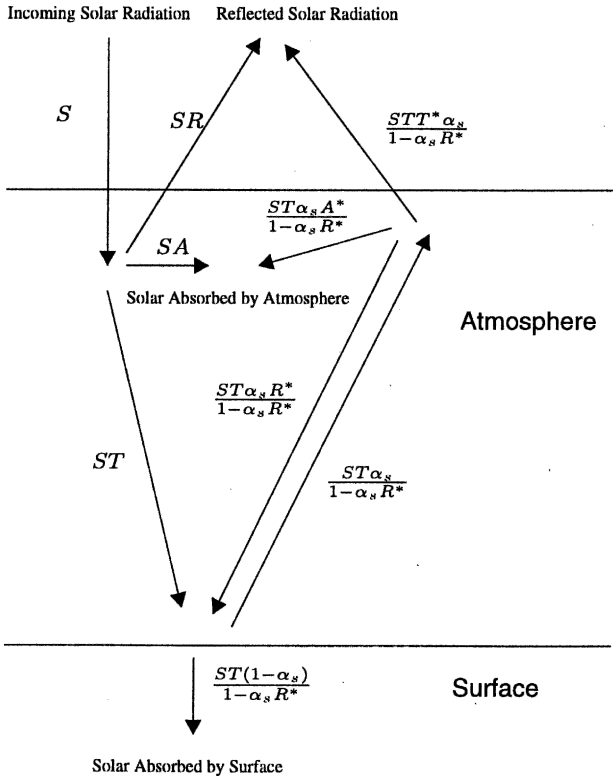

FIG. 2. Possible shortwave radiation pathways. Incoming solar radiation is ultimately reflected to space, absorbed by the surface, or absorbed by the atmosphere.

$$S_s = \frac{ST(1-\alpha_s)}{1-\alpha_s R^*}. \tag{6}$$

The atmospheric shortwave heating (net solar radiation absorbed by the atmosphere) is

$$S_a = SA + \frac{ST\alpha_S A^*}{1-\alpha_s R^*}. \tag{7}$$

To determine the solar optical properties, we need a solar budget with both atmospheric and surface information. Since satellite data provide only TOA information, we use the Langley Surface Radiation Budget (SRB) dataset (Gupta et al. 1999). This dataset uses meteorological data from the International Satellite Cloud Climatology Project (ISCCP) C1 and the Earth Radiation Budget Experiment (ERBE) to compute surface radiative fluxes with a detailed radiative transfer model.

We directly apply annual and zonal average incoming solar radiation and surface albedo (dashed line in Fig. 3) to the model. We multiply the incoming solar radiation by 1.005 to make the global average 342 W m^{-2}. To determine the optical properties of the atmosphere, we assume $A = A^*$, $R = R^*$, and $T = T^*$. This assumption

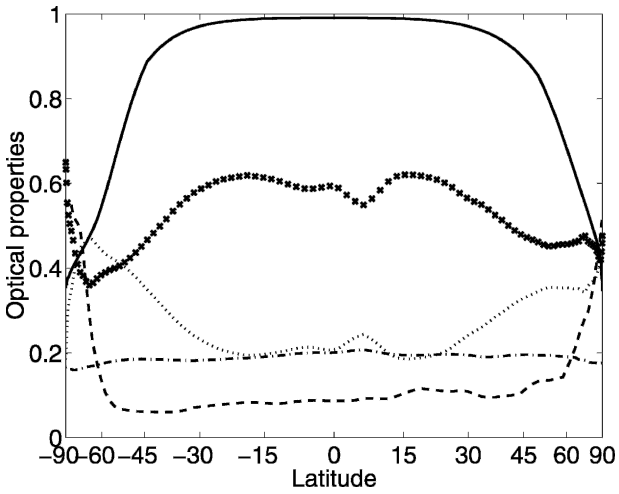

FIG. 3. Shortwave optical properties, A (dashed–dotted), R (dotted), T (×s), and α_s (dashed), derived from SRB data, and calculated longwave emissivity (solid) of the atmosphere [see Eq. (13)].

is necessary since we do not have enough information to solve the radiation budget otherwise. To determine different upward and downward values, we would need data on, for example, the percent of reflected radiation that is reflected by the atmosphere versus by the surface, which is not available from satellite data or normally tabulated in models. Additionally, the computations become significantly more complicated. However, for this version of the model, the solar heating is independent of this assumption since we derive the optical properties such that they generate the correct radiative heating. This approximation is only significant if we vary the atmospheric optical properties, and it is consistent with the complexity of the other model components.

The zonal and annual average reflectivity (R), absorptivity (A), and transmissivity (T) of the atmosphere are calculated based on the atmospheric ($S_{a\mathrm{SRB}}$) and surface ($S_{s\mathrm{SRB}}$) forcing in the SRB dataset:

$$A = \frac{S_{a\mathrm{SRB}}}{S + \alpha_S \dfrac{S_{s\mathrm{SRB}}}{1-\alpha_S}}, \tag{8}$$

$$R = \frac{S_{a\mathrm{SRB}} - SA - S\alpha_s A + SA^2\alpha_s}{S_{a\mathrm{SRB}}\alpha_s - 2SA\alpha_s}, \tag{9}$$

$$T = 1 - A - R. \tag{10}$$

Figure 3 shows the resulting optical parameters. These values are then used in Eqs. (6) and (7) to determine the shortwave heating.

In the real climate system, ice cover and clouds,

which are affected by the temperature, can strongly influence the surface and atmospheric solar absorption. However, in our model, solar heating values are given, based on the specified A, R, T, and α_s values. Thus feedbacks between solar radiation and climate will not be included in our sensitivity studies with this model. The ice–albedo feedback has already been studied extensively in energy balance models, and a cloud feedback algorithm would require much more complexity than is possible in our simple zonal two-layer model (indeed, probably more complexity than is found in most present-day GCMs). Instead, we have chosen to focus on other possible feedbacks, such as the water vapor, lapse rate, and latent and sensible heating feedbacks, described in later sections.

c. Longwave radiation

The possible pathways for longwave radiation are shown in Fig. 4. Terrestrial radiation is emitted by the surface and either absorbed by the atmosphere or lost to space. The atmosphere emits longwave radiation to the surface and to space. The atmosphere absorbs and emits longwave radiation with an emissivity, ϵ, which varies with latitude (Fig. 3). Although the surface absorbs all incoming longwave, it is not a perfect blackbody emitter. Thus, we apply a constant surface emissivity, ϵ_s, to surface emission.

The atmospheric longwave emissivity ϵ is determined from the atmospheric temperature at each grid point, following a calculation similar to that of Pujol and North (2002). We first estimate the saturation water vapor pressure in the boundary layer using an approximation to the Clausius–Clapeyron equation:

$$e_s(T_{\rm bl}) = 2.53 \times 10^{11} e^{-5423/T_{\rm bl}}. \tag{11}$$

The optical depth is determined from the saturation water vapor pressure, e_s, and relative humidity, r,

$$\tau_{\rm lw} = 0.622 k r e_s(T_{\rm bl})/g, \tag{12}$$

where 0.622 is the ratio of the mean molecular weight of water vapor to that of dry air and k is the mass absorption coefficient, which is tuned to produce a reasonable atmospheric emissivity. We assume that relative humidity is constant with both time and latitude.

Finally,

$$\epsilon = 0.3 + 0.7(1 - e^{-\tau_{\rm lw}}). \tag{13}$$

The 0.3 represents the contribution of carbon dioxide and ozone to the atmospheric emissivity (see, e.g., Staley and Jurica 1972), which does not change, while the remainder represents the effects of water vapor. The emissivity varies as a function of latitude and responds (through specific humidity changes) to the model climate.

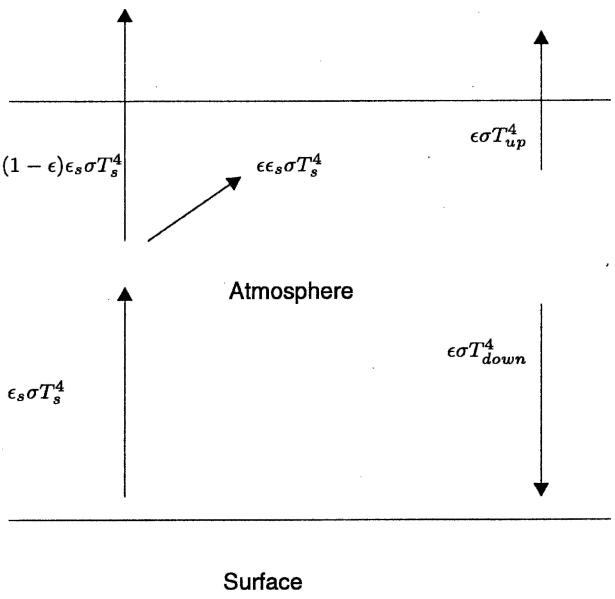

FIG. 4. Possible longwave radiation pathways. Radiation is emitted by the surface and atmosphere. The surface absorbs all incoming longwave radiation, while a portion of the upward longwave radiation passes through the atmosphere to space.

Because the atmosphere emits more radiation outward to space than downward to the surface, the atmosphere effectively emits at two different temperatures:

$$T_{\rm up} = T_a - {\rm lr} \times H_{\rm tm},$$
$$T_{\rm down} = T_a + {\rm lr} \times H_{\rm bm}, \tag{14}$$

where lr is the lapse rate, $H_{\rm tm}$ is the distance from the middle of the layer to the effective height of radiation to space, and $H_{\rm bm}$ is the distance between the middle of the layer and the effective height of radiation to the surface. The heights are constant with latitude and chosen to produce a reasonable longwave energy budget.

Thus, the heating due to longwave radiation is

$$I_a = \epsilon_s \epsilon \sigma T_s^4 - \epsilon \sigma T_{\rm up}^4 - \epsilon \sigma T_{\rm down}^4, \tag{15}$$

$$I_s = \epsilon \sigma T_{\rm down}^4 - \epsilon_s \sigma T_s^4. \tag{16}$$

The longwave radiation, in contrast to the shortwave heating, varies with the climate. For example, because we determine the atmospheric emissivity using the boundary layer temperature, the model includes a simplified water vapor feedback. Changes in lapse rate will also affect the longwave fluxes. While the lapse rate, temperature, and emissivity of the atmosphere are allowed to vary, the heights of emission to space, $H_{\rm tm}$, and to the surface, $H_{\rm bm}$, are tuned to match the ob-

served longwave flux and thus do not change with the climate. In reality, we expect these heights to change as the longwave absorber (water vapor) concentration changes. Thus, the model does not completely represent the water vapor feedback, but the level of approximation is consistent with the rest of the model.

d. Latent and sensible heat fluxes

The latent and sensible heat fluxes from the surface to the atmosphere are specified by the bulk equations

$$F_l = \rho_a C_D u L \frac{0.622[e_s(T_s) - re_s(T_{\rm bl})]}{P}, \qquad (17)$$

$$F_s = \rho_a C_D u C_p (T_s - T_{\rm bl}), \qquad (18)$$

where ρ_a is the surface air density, C_D is the drag coefficient, L is the latent heat of vaporization, P is the surface pressure, and C_p is the specific heat capacity. The relative humidity, r, is held constant, and the specific humidity has been approximated as the ratio of the mean molecular weight of water vapor to that of dry air (0.622) times the ratio of the partial pressure of water vapor to that of air. The surface wind, u, is obtained from the Goddard Space Flight Center Data Assimilation Office's (DAO) monthly mean dataset (Schubert et al. 1993).

The latent heating (but not sensible heating) is weighted by the fraction of ocean in a latitude band because most evaporation occurs over the ocean. In addition, the latent heat flux is constrained to be positive. The model assumes that all water vapor is evaporated and condensed at the same latitude. Thus, this parameterization includes no explicit meridional latent heat transport. To produce a reasonable meridional temperature gradient, other components of the model, such as the atmospheric eddy transport parameterization and Hadley cell adjustment, presented in the next section, must compensate for the lack of latent heat transport. This compensation may result in local (i.e., existing within a particular latitude range) errors in the energy budget.

e. Dynamics parameterizations

For the surface layer, the effect of dynamics depends on whether the surface is ocean or land. On land, there is no transport of heat, and thus the heat tendency due to surface transport, D_s, is zero. For ocean surfaces, D_s represents the transport of heat by ocean currents. The issue is complicated by the fact that most latitude bands include both land and ocean. For simplicity, surface layer dynamics are approximated as a diffusive process with a latitude-varying diffusivity, $D_0(\phi)$:

$$D_s = \frac{\partial}{\partial x} D_0(\phi)(1 - x^2) \frac{\partial T_s}{\partial x}, \qquad (19)$$

where x is sin ϕ.

The diffusivity depends on three values: the latitude, the fraction of ocean in a latitude band, and a specified latitude-independent value, D_{s0}. We use the parameterization in the Global Environmental and Ecological Simulation of Interactive Systems (GENESIS) version 2 slab ocean model (Thompson and Pollard 1997). First, D_{s0} is multiplied by a factor based on the fraction of ocean at a given latitude. If the ocean fraction is less than or equal to 0.75, the diffusion coefficient is unmodified. If the fraction is greater than 0.75, the factor decreases linearly from 1 at 0.75 to 0.1 for an entirely ocean-filled latitude. This modification reduces the transport in latitudes that are primarily or entirely ocean, where the transport is not efficient. Next, this resulting value is multiplied by a factor dependent on the latitude. This factor is 1 if the latitude is equatorward of 20° and 0.3 if poleward of 30°, with a linear decrease between the two latitudes. This modification enhances the equatorial transport compared with transport farther poleward. This parameterization was developed to match the observed ocean transport (Thompson and Pollard 1997).

In the atmosphere, the dynamics parameterization represents the effects of the mean circulation and eddies on the meridional transport of heat. Generally, the mean circulation plays the dominant role in the Tropics, while eddies are the main dynamical transport mechanism in middle and high latitudes.

1) EDDY TRANSPORT

The change in temperature due to eddies is calculated from the meridional convergence of heat flux:

$$D_a = -\frac{1}{a}\frac{\partial}{\partial \phi}(\overline{T_a v}). \qquad (20)$$

The meridional eddy heat flux calculation follows the Stone (1974) parameterization. Stone uses Eady's (1949) two-layer model to calculate correlations between the temperature and meridional velocity based on small-amplitude growing baroclinic instabilities. He determines the amplitude of these perturbations by assuming that they are limited by nonlinear effects to attain the amplitude of the mean flow. The meridional eddy heat flux is related to both the local meridional temperature gradient and the vertical average of tropospheric static stability:

$$\overline{T_a v} = -0.144 \frac{g H_e^2}{f^2 T_a a^2} \left[\frac{g}{T_a}(\Gamma - \mathrm{lr})\right]^{1/2} \left|\frac{\partial T_a}{\partial \phi}\right| \frac{\partial T_a}{\partial \phi}, \qquad (21)$$

where a is the radius of the earth, g the acceleration due to gravity, f the Coriolis parameter, and H_e the scale height. Our inclusion of an independently calculated static stability in this calculation differs from the common treatment of eddy transport in most energy balance models. Thus, our model allows for feedbacks between the lapse rate and meridional heat flux.

This parameterization explicitly includes only sensible heat transport; latent heat transport is excluded. However, latent heat transport does contribute to the earth's actual heat transport. Thus, we tune the magnitude of H_e to account for the total heat transport and obtain a reasonable total atmospheric heat transport.

2) HADLEY TRANSPORT

The Hadley transport parameterization is applied as an adjustment to the atmospheric temperature after each time step. In effect, transport by the Hadley cell immediately responds to changes in atmospheric temperature. The adjustment is based on the inviscid Hadley cell theory of Held and Hou (1980), described briefly here.

Each hemisphere is divided into two regions. The temperature in the region near the equator is affected by the Hadley circulation, while the temperature poleward of this region is not modified. The regions are bounded by a critical latitude, ϕ_c, which is calculated as part of the Hadley cell adjustment.

To determine the temperature in the region near the equator, we assume that the upper (poleward) branch of the Hadley cell conserves angular momentum from the equator to the critical latitude (the inviscid limit). Thus, the zonal wind in this region is

$$\Omega a \frac{\sin^2\phi}{\cos\phi},$$

with the zonal wind equal to zero at the equator. The temperature within the Hadley cell is assumed to be in thermal wind balance with the angular-momentum-conserving wind:

$$\frac{T_a(0) - T_a(\phi)}{T_{a0}} = \frac{\Omega^2 a^2}{gH_t} \frac{\sin^4\phi}{2\cos^2\phi}, \tag{22}$$

where T_{a0} is the mean temperature, Ω the rotation rate, and H_t the height of the troposphere. Note that for simplicity, the height is specified as a constant in this model, although we would expect it to vary as the temperature in the Tropics changes.

Poleward of the critical latitude, the meridional wind goes to zero, and the temperature is just the temperature already determined by the model at each time step, before Hadley cell adjustment is applied, T_E. This value corresponds to the "radiative equilibrium" value discussed in Held and Hou (1980), but our value includes the effects of midlatitude eddies and latent and sensible heating as well. The temperatures at the equator and the critical latitude are found by requiring that the Hadley cell solution and the previous model solution match at the critical latitude,

$$T_a(\phi_c) = T_E(\phi_c), \tag{23}$$

and that temperature is conserved within the Hadley cell (the Hadley circulation cannot add or remove heat from the atmosphere; can merely redistribute it:

$$\int_{\phi_{\mathrm{ITCZ}}}^{\phi_c} T_a \cos\phi \, d\phi = \int_{\phi_{\mathrm{ITCZ}}}^{\phi_c} T_E \cos\phi \, d\phi, \tag{24}$$

where ϕ_{ITCZ} is the latitude that separates the northern and southern cells. A final constraint is that the southern and northern cells must have the same temperature at the equator.

These equations are solved using an iterative process. Equation (23), combined with Eq. (22), specifies a temperature profile, assuming that the critical latitude is given. Each grid point is used as a critical latitude in Eq. (24) to determine which best satisfies the conservation of temperature constraint, assuming that ϕ_{ITCZ} is 0 (i.e., the ITCZ, or boundary between the northern and southern cells, is at the equator). Note that this calculation is performed for both the northern and southern cells separately. Since the hemispheres may have different average temperatures, the Hadley-adjusted atmospheric temperature is not necessarily symmetric about the equator. Furthermore, the critical latitude may be at different latitudes in the Northern and Southern Hemispheres.

We next move ϕ_{ITCZ} north or south incrementally by one grid point and repeat the Eq. (24) calculations until the difference between the equatorial temperatures computed for the northern and southern cells is minimized. This minimization procedure for two hemispheres is based on notes from a course by Isaac Held.

The final Hadley-adjusted solution for the air temperature is the Hadley cell solution equatorward of the critical latitude and the unmodified model solution poleward of the critical latitude. To prevent an instability in the model due to oscillations of the edges of the Hadley cell from one grid point to another, we relax the model temperature to the Hadley cell temperature with a time constant, which depends on the total number of grid points. The resulting temperature is not sensitive to the specific time constant used.

This temperature adjustment accounts for a complicated mixture of energy transport by the Hadley cell,

including sensible and latent heat and potential energy transport. Some of these, sensible and latent heat transport, are actually equatorward in the cell. This parameterization represents the net result of these Hadley circulation heat transports on the temperature profile. Other effects of the Hadley cell, such as changes in water vapor concentration, are not included. Latent heat released during vertical motions is already roughly accounted for in the latent heat parameterization, though, as discussed earlier, the evaporation and condensation unrealistically occur at the same latitude.

3. Comparison of model climate with observations

Before examining the sensitivity of the model, we first demonstrate that it produces a reasonable present climate. The parameter values used to obtain this climate are summarized in Table 1. Model variables $H_{\rm tm}$, $H_{\rm bm}$, H_l, H_m, r, C_D, ϵ_s, k, D_{s0}, H_e, and H_t have been tuned to obtain a realistic climate; variables calculated by the model are listed in Table 2. We compare the main variables, the atmospheric and surface temperatures, as well as some intermediate results to annual and zonal averages of observations.

Figure 5 compares the modeled surface temperature with estimates from the DAO (Schubert et al. 1993) and SRB (Gupta et al. 1999) datasets. The difference between the datasets provides an indication of uncertainties in these surface temperature data. Our model shows good agreement with these surface temperatures, though some details are lacking. For example, the observed slight decrease in temperature found at the equator is related to deep convection, which is not included in our simple model. The model surface temperature is higher than those derived from observations in high southern latitudes because the surface of Antarctica is significantly above sea level. Our model does not include topography, and, therefore, our surface temperatures all correspond to sea level values. In addition, the SRB shortwave heating may be too high in

TABLE 1. Independent variables. Values are listed for those that are constant with latitude.

Variable	Description	Value	Units
N	Number of grid points	200	—
ϕ	Latitude		degrees
Δt	Time step	10	s
δ	Allowed error	5×10^{-8}	K s^{-1}
C_s	Heat capacity of surface	4×10^{7}	J m^{-2}K^{-1}
C_a	Heat capacity of atmosphere	9.6×10^{5}	J m^{-2}K^{-1}
Γ	Dry-adiabatic lapse rate	9.8	K km^{-1}
H_l	Scale height for lapse rate	12	km
r	Relative humidity	0.8	—
H_m	Height of middle of atmosphere layer	3.6	km
S	Incoming solar radiation		W m^{-2}
α_s	Surface albedo		—
R	Reflection of atmosphere		—
T	Transmission of atmosphere		—
A	Absorption of atmosphere		—
ϵ_s	Longwave surface emissivity	0.975	—
k	Mass absorption coefficient for water	0.03	m^2 kg^{-1}
g	Acceleration due to gravity	9.8	m s^{-2}
$H_{\rm tm}$	Top to middle atmospheric layer distance	2	km
$H_{\rm bm}$	Bottom to middle atmospheric layer distance	2.6	km
σ	Stefan–Boltzmann constant	5.67×10^{-8}	W m^{-2} K^{-4}
C_D	Drag coefficient	0.0011	—
ρ_a	Surface air density	1.3	kg m^{-3}
L	Latent heat of vaporization	2.5×10^{6}	J kg^{-1}
P	Surface pressure	1.013×10^{5}	Pa
u	Surface wind speed		m s^{-1}
C_p	Specific heat capacity	1004	J kg^{-1} K^{-1}
D_{0s}	Diffusion coefficient of surface	2.2×10^{-8}	W m^{-2} K^{-1}
a	Radius of the earth	6.37×10^{6}	m
f	Coriolis parameter		s^{-1}
H_e	Scale height for Stone heat flux	28 000	m
Ω	Rotation rate	7.2722×10^{-5}	s^{-1}
H_t	Height of troposphere for Hadley cell	17 000	m

TABLE 2. Dependent variables.

Variable	Description	Units
T_a	Atmospheric temperature	K
T_s	Surface temperature	K
S_a	Solar radiation absorbed by atmosphere	W m^{-2}
S_s	Surface shortwave (SW) heating	W m^{-2}
S_{TOA}	TOA SW heating	W m^{-2}
I_s	Surface longwave (LW) heating	W m^{-2}
I_a	Atmospheric LW heating	W m^{-2}
I_{TOA}	TOA LW heating	W m^{-2}
F_l	Latent heat	W m^{-2}
F_s	Sensible heat	W m^{-2}
D_a	Atmospheric heat transport tendency	W m^{-2}
D_s	Ocean transport tendency	W m^{-2}
lr	Lapse rate	K km^{-1}
T_{bl}	Boundary layer temperature	K
ϵ	Emissivity of atmosphere	—
T_{up}	Atmospheric upward emission temperature	K
T_{down}	Atmospheric downward emission temperature	K
T_E	Held–Hou "radiative equilibrium" temperature	K

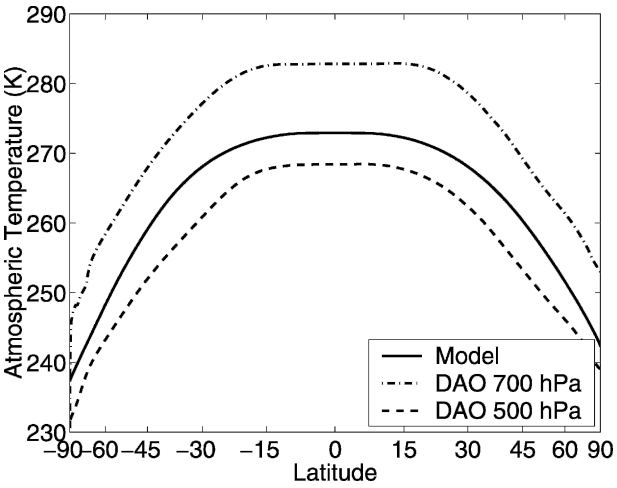

FIG. 6. Atmospheric temperature of the model (solid) compared with DAO 500- (dashed) and 700-hPa (dashed–dotted) atmospheric temperature. Based on the height of the model atmosphere, the pressure is about 650 hPa.

this region (see the comparison with ERBE data in Fig. 7). We have specifically tuned the model to have a global average surface temperature of 288 K. Thus, regions with low temperature (e.g., Northern Hemisphere Tropics) are balanced by regions of high temperature (Northern Hemisphere middle and high latitudes). On the global average, the modeled surface temperature is 288.3 K, in agreement with accepted values. The SRB and DAO datasets are slightly colder: 287.5 and 287.0 K, respectively.

The atmospheric temperature (Fig. 6) also agrees fairly well with the DAO data. The atmospheric temperature does not correspond exactly to a specific pressure or height, so comparisons are difficult. However, the general profile is approximately correct. The Hadley circulation serves to decrease atmospheric temperature gradients in the Tropics, resulting in a reasonably flat temperature. The circulation also transports heat from the Southern Hemisphere to the Northern Hemisphere.

The TOA (Fig. 7, dashed line) longwave budget agrees fairly well with ERBE S-4G Scanner (SC) 2.5° zonal average data (Barkstorm et al. 1989), except for differences related to water vapor and cloud distributions. In the Tropics, the outgoing longwave radiation is

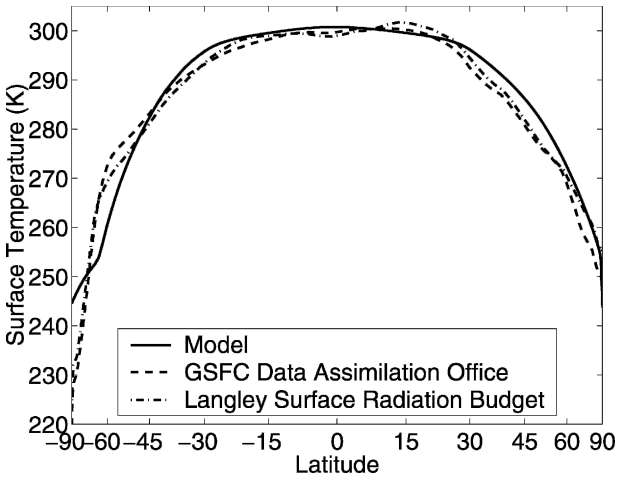

FIG. 5. Surface temperature of the model compared with DAO and SRB data.

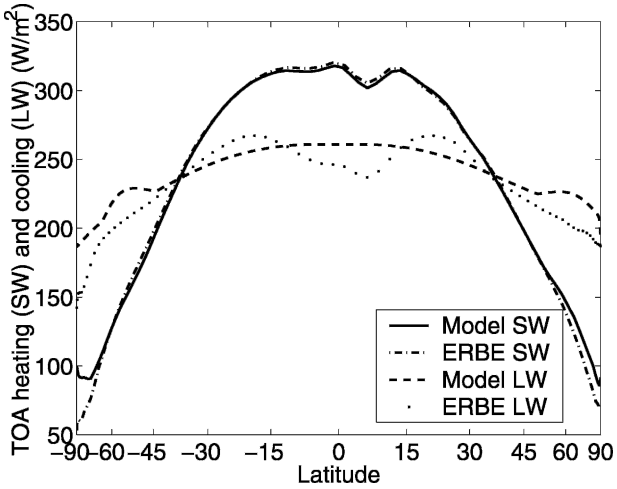

FIG. 7. TOA shortwave heating and outgoing longwave in the model compared with ERBE observations.

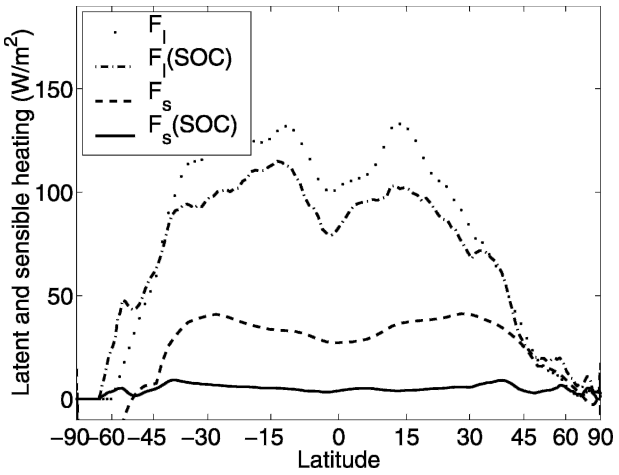

FIG. 8. Latent and sensible heating transferred from the surface to the atmosphere compared with the Southampton Oceanography Centre Global Air–Sea Heat and Momentum Flux Climatology (Grist and Josey 2003).

decreased by deep convective clouds. These clouds are not present in the subtropics where subsidence maintains a clear sky and more effective longwave cooling. Similarly, cloudiness in the mid- and high latitudes decreases outgoing longwave radiation. These effects are not included in the model; thus the modeled TOA outgoing longwave is too large in the Tropics and small in the subtropics. Globally, the model outgoing longwave radiation is a little high compared to ERBE data. The shortwave budget (Fig. 7, solid line) matches the ERBE data fairly well, though this is not entirely surprising given that the SRB data are partially derived from the ERBE data. The difference at high latitudes is due to the difficulty in obtaining solar parameters at high zenith angles and problems in the SRB radiation calculations.

Figure 8 shows the latent and sensible heat fluxes from the surface to the atmosphere. Positive values indicate a loss of heat from the surface. The model results are compared with the adjusted Southampton Oceanography Centre (SOC) Global Air–Sea Flux Climatology (Grist and Josey 2003). This dataset uses data from voluntary observing ship reports in the Comprehensive Ocean–Atmosphere Dataset, with adjustments due to an inverse analysis using World Ocean Circulation Experiment (WOCE) transect data and global net flux constraints. The global mean net heat flux of this dataset is 2 W m^{-2} out of the ocean. Our model results correspond well to this data, with latent heat peaks in subtropics and less exchange at the equator. The sensible heat values are higher than fluxes in this dataset. However, the SOC sensible heat data only include oceanic sensible heat fluxes and thus neglect land fluxes. Our modeled global average values are reasonable compared with the Kiehl and Trenberth (1997) values (Table 3).

The longwave emission, sensible heat, and latent heat calculations are heavily dependent on the lapse rate (Fig. 9). In comparison with lapse rates averaged over different pressure intervals from the DAO data, the model correctly produces two different regions of lapse rate behavior, flatter in the Tropics and subtropics and steeper in high latitudes. The atmosphere cannot be described by a single lapse rate throughout the troposphere since it changes with height (note the spread in observed lapse rates when different pressure ranges are used). However, the overall pattern is reasonable given the simplicity of our model.

The effect of eddies is shown in Fig. 10. Results from Trenberth and Caron (2001) are shown for comparison. Trenberth and Caron (2001) calculate atmospheric heat transport from the National Centers for Environmental Prediction–National Center for Atmospheric Research (NCEP–NCAR) reanalysis. They then determine ocean heat transport from ERBE TOA radiative fluxes and the calculated atmospheric fluxes. Our modeled atmospheric transport is larger than the modeled oceanic transport and peaks at the correct latitude. However, it is about half the strength of the observed peak. Trenberth and Caron (2001) obtain a Northern Hemisphere atmospheric transport peak of 5.0 ± 0.14 PW, while we obtain a maximum of 2.6 PW. Note that our model results exclude transport due to the Hadley circulation and thus are low in the Tropics. The ocean transport is about the correct magnitude but peaks

TABLE 3. Globally averaged model values and observed values from Kiehl and Trenberth (1997).

Variable	Model value	Observed value
Surface temperature (K)	288	288
TOA SW heating (W m^{-2})	242	235
TOA LW heating (W m^{-2})	−242	−235
Latent heating (W m^{-2})	79	78
Sensible heating (W m^{-2})	22	24
Incoming solar (W m^{-2})	342	342
Planetary albedo	0.29	0.31
Fraction of incoming solar absorbed by atmosphere	0.20	0.20
Fraction of incoming solar absorbed by surface	0.50	0.49
Total LW absorbed by surface (W m^{-2})	316	324
Total LW emitted by surface (W m^{-2})	388	390
Total LW absorbed by atmosphere (W m^{-2})	352	350
Total LW emitted by atmosphere (W m^{-2})	522	519

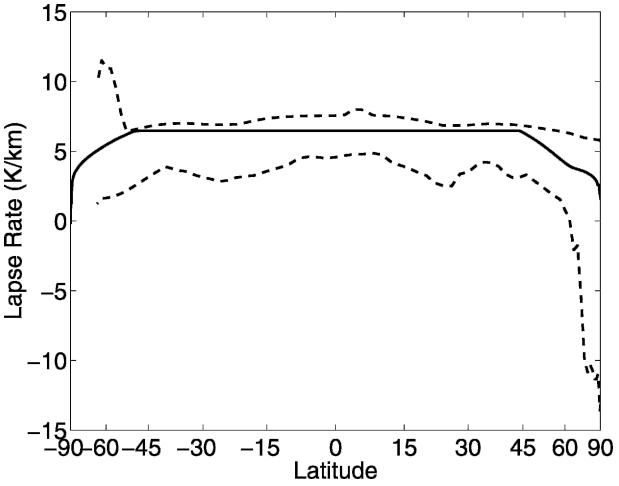

FIG. 9. Lapse rate in the model. The dashed lines indicate the range of tropospheric lapse rates calculated from the DAO data using different pressure intervals.

poleward of Trenberth and Caron's (2001) transports, especially in the Northern Hemisphere.

The bottom panel in Fig. 10 illustrates that the Trenberth and Caron net column transport is larger than our modeled transport. Our model is energetically consistent; the net transport required by the TOA radiative budget is essentially the same as the transport obtained from the dynamical parameterizations. Thus, the differences between the model results and Trenberth and Caron (2001) are based on discrepancies in the latitudinal variation in net TOA radiation. First, Trenberth and Caron use a revised version of the ERBE data; thus it is not exactly the same as the ERBE data shown earlier, and we expect differences between the resulting transports. Also, the model uses essentially the ERBE shortwave radiation, but the longwave radiation pattern is locally different. For example, the modeled outgoing longwave radiation is too high in the Tropics and too low in the subtropics compared with ERBE (Fig. 7). As a result, less heat needs to be transported from the Tropics to subtropics to balance the net TOA radiation. Thus, the magnitude of the transport in the model is less that that obtained by Trenberth and Caron (2001) due to errors in the outgoing longwave radiation calculation, especially the simplicity of the water vapor distribution. The lack of meridional latent heat transport may also be responsible for some of the error as well.

Table 3 provides global values for some of these variables in comparison with the estimates of Kiehl and Trenberth (1997). The shortwave budget, which is entirely specified by the SRB dataset, is within the uncertainty of the known values, though the model has a lower planetary albedo. Global average latent and sensible heat fluxes are quite close to the Kiehl and Trenberth (1997) averages. The longwave budget differs slightly but not significantly. Within the uncertainty of these global averages, the model produces a quite reasonable climate.

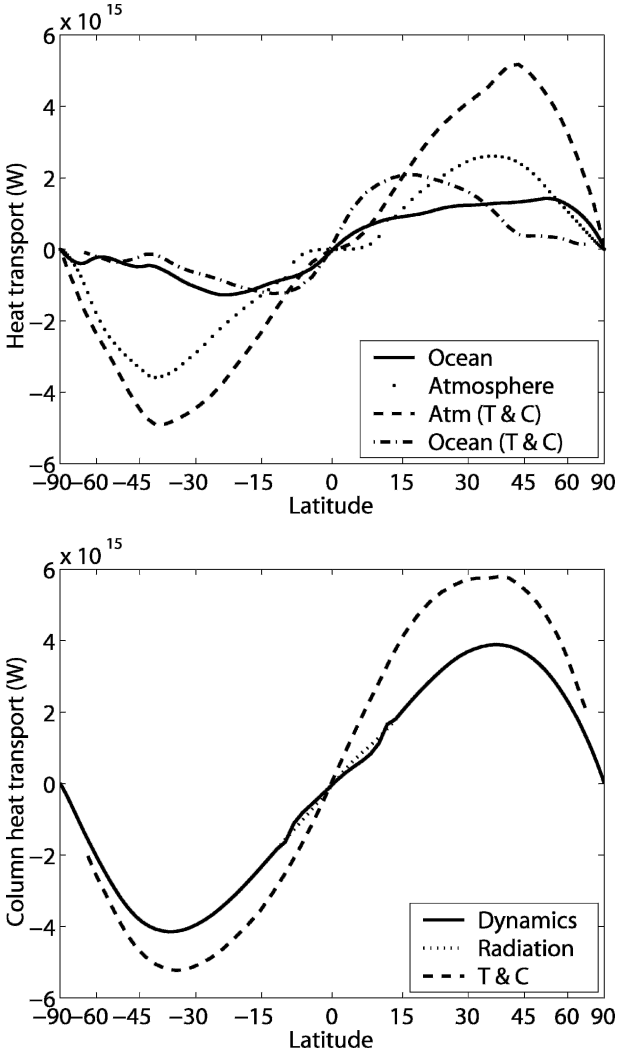

FIG. 10. Northward heat transport by the model ocean and atmospheric eddies compared with Trenberth and Caron (2001) estimates. The top figure shows the individual components, while the bottom figure compares the column transport calculated by the model with that required by the modeled TOA radiation budget. Note that transport by the Hadley circulation parameterization is excluded.

4. Feedbacks and climate sensitivity

A strength of this model is its inclusion of feedbacks related to the vertical structure of the atmosphere. In this section, we present two examples of sensitivity studies that utilize this strength. In so doing, we have allowed parameters, such as solar constant and eddy

diffusivity, to vary over a large range of values. Of course, we do not mean to imply that the resulting changes are realistic, since we expect many other feedbacks to become dominant at such extremes, and our parameterizations, which have been tuned using the present climate, will no longer be valid. However, we study the behavior of the system in extreme cases to emphasize and illustrate model feedbacks that might not be as apparent from smaller changes.

a. Solar constant

A traditional sensitivity experiment is to vary the global average incoming solar radiation. The solar constant was different from the present-day value in the past, and the variability of the solar output has been suggested by many as a cause of past climate change. Additionally, changes in the solar constant are often used as proxies for forcing caused by increased greenhouse gases.

We alter the magnitude of the solar heating by multiplying the incoming solar radiation by a range of constants. Figure 11 shows the resulting changes in global average surface and atmospheric temperatures. A 2% increase in the solar constant results in a surface temperature warming of 1.0 K, while the atmospheric temperature increases by 1.3 K. These values are lower than those commonly cited for a 2% change. For example, Hansen et al. (1984) obtain a 4-K change in a GCM experiment. The Intergovernmental Panel on Climate Change (IPCC) report (Houghton et al. 2001) gives a range of climate sensitivity to a doubling of CO_2 (similar in forcing to a 2% solar increase) as 1.5–4.5 K.

The sensitivity of our model is less than other sensitivity estimates. There are a few specific reasons for the lower sensitivity. First, although the model includes a simple water vapor feedback, it omits any feedbacks related to the vertical distribution of water vapor. Models that do allow the vertical distribution of water vapor to change (e.g., Wetherald and Manabe 1975; Hansen et al. 1984) suggest that this positive feedback largely balances the negative lapse rate feedback. Our model includes the lapse rate feedback but omits this vertical water vapor feedback. In addition, in our model, the lapse rate feedback is negative everywhere, while Wetherald and Manabe (1975) and Hansen et al. (1984) obtain a positive feedback in high latitudes where the lapse rate increases with the solar constant. Thus, our global average lapse rate feedback may be too strong. The net effect is a large negative feedback related to the lapse rate. When the lapse rate feedback is omitted from the model, the sensitivities of the atmospheric and surface temperatures for a 2% solar constant increase are larger (1.7 K for both), corresponding to the low end of the IPCC report sensitivity. The negative lapse rate feedback is described in more detail in a later section.

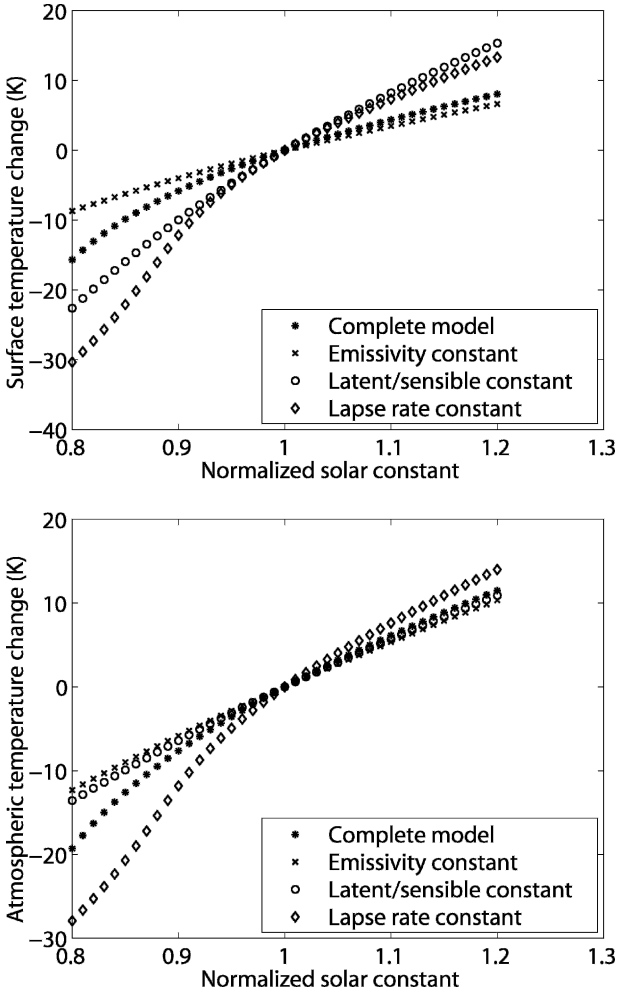

FIG. 11. Change in global average (top) surface and (bottom) atmospheric temperature as a function of solar constant relative to the present-day amount. Atmospheric longwave emissivity is a positive feedback on both the surface and atmospheric temperatures, while the lapse rate feedback is negative. The latent and sensible heat feedbacks increase the atmospheric temperature changes and decrease the surface temperature changes.

Our model further underestimates the water vapor feedback by using constant heights for the longwave atmospheric emission upward to space and downward to the ground. The heights are specified and do not vary as a function of water vapor. In reality, these heights would be affected by the amount of water vapor in the atmosphere. If the amount of water vapor increases (due to rising atmospheric temperatures), there would be more absorbers in the atmosphere, so the height of downward emission decreases, leading to increased emission toward the ground. Similarly, the height of

upward emission increases, reducing emission to space and further enhancing the greenhouse effect. The net effect is a positive feedback on the atmospheric temperature change, which is not incorporated into our model. In addition, other longwave processes (e.g., the effect that clouds have on the longwave budget) are not included in this simple model. Thus, interactions between some feedbacks, such as the relationship between the cloud-top feedback and the lapse rate feedback, described by Ramanathan (1977), are omitted.

Another reason our modeled sensitivity is low is the lack of any solar radiation feedback. Since the surface albedo is specified, the model omits the positive ice–albedo feedback. In addition, the solar optical properties of the atmosphere do not change in response to climate, so feedbacks related to clouds are not included. These longwave and shortwave factors contribute to the low climate sensitivity of our model. However, keeping these limitations in mind, our model can still be useful in exploring the feedbacks that are included and understanding relationships among different climate components.

The temperature changes more rapidly as the solar constant is decreased than as the solar constant is increased. Decreasing the solar constant by 20% decreases the surface temperature by 15.7 K (5%), while increasing the solar constant by 20% results in warming of 8.1 K (3%). As the atmospheric temperature changes, the resulting emissivity changes are larger when the temperature decreases than when it increases. Thus, the emissivity feedback, discussed in more detail below, is stronger for a decrease in solar constant than for an increase.

To understand the feedbacks responsible for the magnitude and nonlinearity of the sensitivity to solar constant, we repeat the calculations while holding various model terms constant. We examine three feedbacks within the model: the emissivity feedback, latent and sensible heat feedback, and lapse rate feedback. Figures 11 through 13 show different aspects of the results. Figure 11 shows the temperature changes as a function of solar constant. Figures 12 and 13 show the responses of different model components (emissivity, lapse rate, boundary layer temperature, and latent and sensible heat fluxes) to these solar constant changes. To better study the effects of feedbacks on these components, we plot them as a function of global average atmospheric temperature rather than solar constant. In this way, we eliminate differences between versions of the model based solely on different climate sensitivities to incoming solar radiation. For example, from Fig. 11b, the atmospheric temperature changes more in the case where the lapse rate feedback is omitted (1.7 K for a

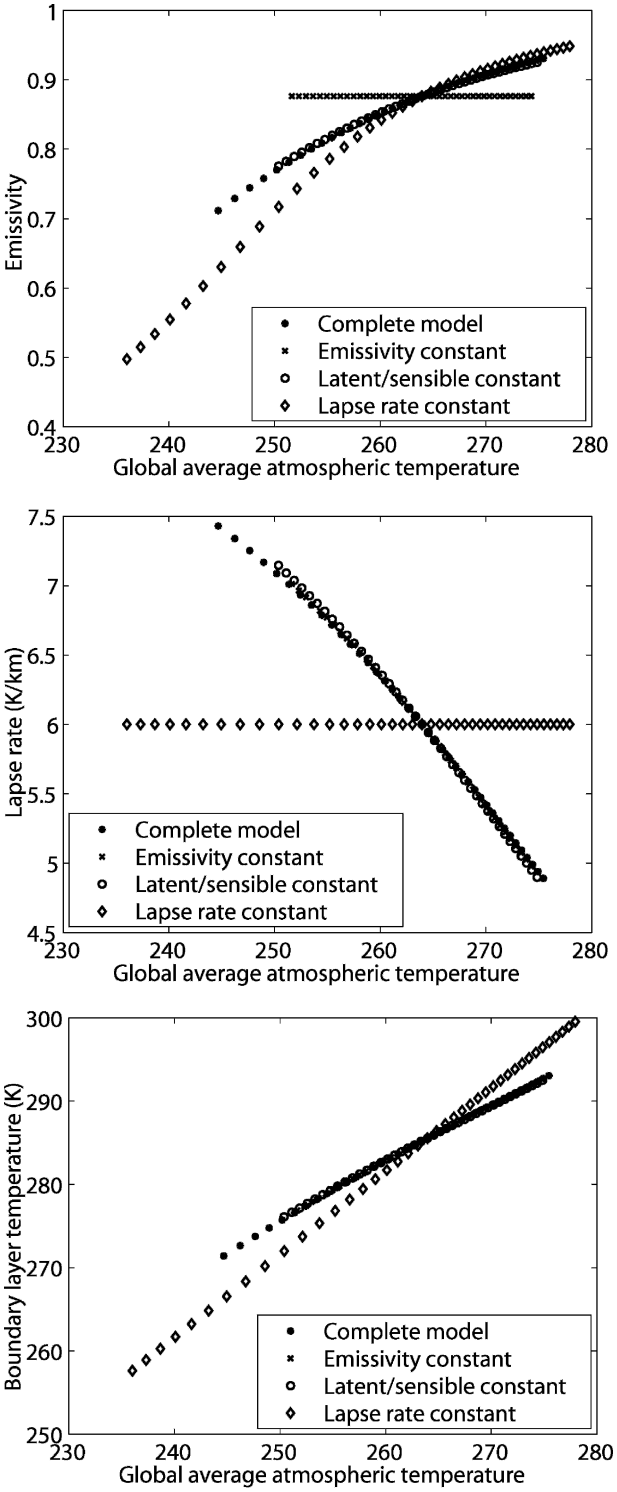

FIG. 12. Global average (top) emissivity, (middle) lapse rate, and (bottom) boundary layer temperature as a function of global average atmospheric temperature. Emissivity and boundary layer temperature increase with atmospheric temperature, while the lapse rate decreases. The changes are similar for the different versions of the model; however, the lapse rate feedback significantly affects the emissivity and boundary layer temperature changes.

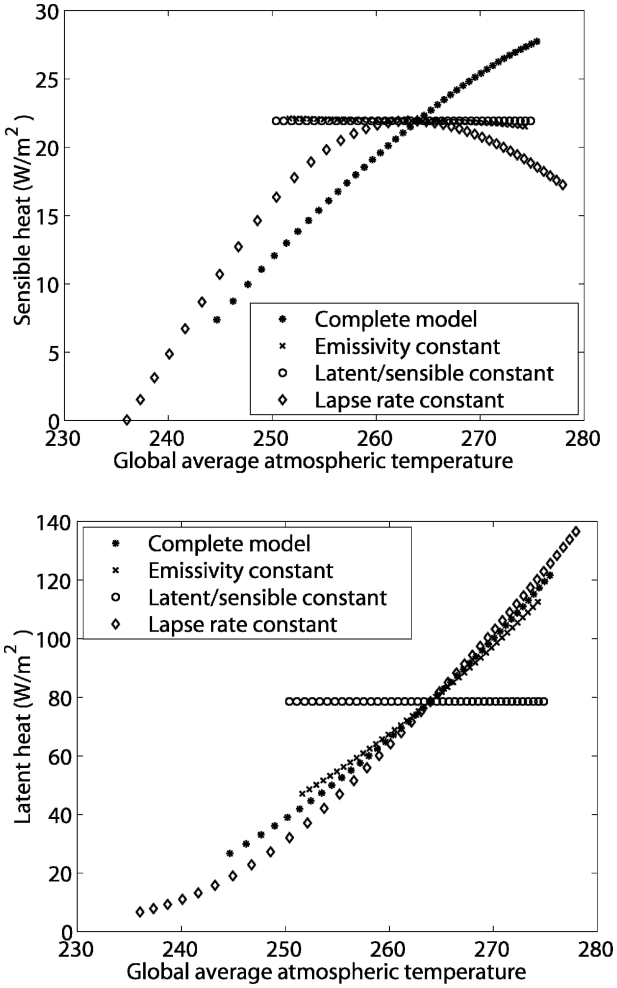

FIG. 13. Global average (top) sensible and (bottom) latent heating as a function of global average atmospheric temperature. Latent and sensible heating fluxes increase with increasing temperature, except in the case omitting the lapse rate feedback. Sensible heating is very sensitive to the emissivity and lapse rate feedbacks, while the latent heating response is not as varied.

2% solar constant increase) than it does in the full model case (1.3 K). Thus, we expect atmospheric emissivity to increase more as the solar constant increases in the constant lapse rate version as opposed to in the full model, simply because the atmospheric temperature increases faster. However, Fig. 12a shows that the emissivity does not have the same relationship to the atmospheric temperature in the constant lapse rate case as in the other cases. The difference between these lines points to a feedback between the lapse rate and atmospheric emissivity (described later), which would not be as evident in an emissivity versus solar constant plot. This diagnostic technique allows us to isolate specific effects and interactions within the model. Note that we use the global average atmospheric temperature as a proxy for the overall climate state. We could have also used the surface temperature; however, the atmospheric temperature has a more direct effect on the emissivity, lapse rate, and boundary layer temperature.

1) WATER VAPOR FEEDBACK

We first examine the behavior of the emissivity/water vapor feedback. Holding the atmospheric longwave emissivity constant (×s in Fig. 11) is equivalent to eliminating the water vapor feedback. By comparing these results with the full model results (asterisks), we see that the water vapor feedback is a positive feedback for both the surface and atmosphere (i.e., the climate excluding this feedback changes less than the climate with the water vapor feedback included). This occurs because a warmer temperature results in a higher water vapor content and thus higher emissivity (see Fig. 12a). The higher emissivity enhances the greenhouse effect and further increases the temperature. Without the water vapor feedback, the change in surface temperature is only about 75% of the change when the model includes the feedback. Our water vapor feedback is not as effective as water vapor feedbacks in other models. For example, Hansen et al. (1984) obtain about 60% of the temperature change in a simplified GCM when the water vapor feedback is excluded, and Manabe and Wetherald (1967) obtain about half of the change in a radiative–convective model. However, given the simplicity of our water vapor feedback, which is solely based on a constant relative humidity and lacks the complex distribution of water vapor based on atmospheric dynamics, our feedback is reasonably close to that found in more complicated models.

We expect that latent heating will not increase as quickly with the solar constant when the emissivity feedback is excluded because the temperature does not increase as quickly, resulting in a smaller saturation humidity change. However, another interaction also occurs, as shown by a comparison of the asterisks and ×s in Fig. 13. Since atmospheric temperature has a one-to-one correspondence with the boundary layer temperature (asterisks and ×s in Fig. 12c) and thus boundary layer humidity, boundary layer differences cannot be responsible for the differences between the asterisk and × lines in Fig. 13. That is, for a given global average atmospheric temperature, the second terms in Eqs. (17) and (18) are the same for the versions of the model with and without the emissivity feedback. Thus, the reduced change in latent heat (as a function of atmospheric temperature) when compared to the full model case is a result of a decreased change in surface temperature, that is, the surface temperature does not increase as quickly with increased atmospheric temperature as it

does when the emissivity is allowed to vary. This process occurs in conjunction with the reduced saturation humidity change previously discussed.

The emissivity feedback also affects the sensible heat flux. When the emissivity feedback is omitted, the global average sensible heat flux actually decreases slightly as the solar constant increases. Both the boundary layer and surface temperatures are increasing. However, the boundary layer temperature increases faster than the surface temperature; thus the sensible heat flux decreases in the no emissivity feedback case.

2) LATENT AND SENSIBLE HEAT FEEDBACK

The change in latent and sensible heat fluxes is a significant part of the climate response to an imposed forcing. These surface–atmosphere fluxes change in response to forcing, with implications for the hydrological cycle, and they contribute to the modification of the surface budget as well. Ramanathan (1981) demonstrates the importance of surface–atmosphere interactions in determining the climate response to changes in CO_2.

The circles in Fig. 11 show that the latent and sensible heating feedback in our model is negative at the surface and positive in the atmosphere. In a warmer climate, more water evaporates from the surface. Thus, the surface warms less rapidly, and the atmosphere warms more rapidly, as the solar constant is increased. In addition, as the climate warms due to solar constant changes, the difference between the surface temperature and boundary layer temperature increases. (Although the atmospheric temperature increases more rapidly than the surface temperature, lapse rate decreases reduce the increase in boundary layer temperature. When the lapse rate feedback is eliminated, as shown by the diamonds in Fig. 12c, the boundary layer temperature increases faster.) This increased temperature difference increases both latent and sensible heat transfer (Fig. 13), further contributing to both the negative surface feedback and the positive atmospheric feedback. This feedback almost halves the surface temperature response. When the feedback is eliminated, the surface temperature change is about 80% larger than in the complete model.

3) LAPSE RATE FEEDBACK

Finally, we explore the lapse rate feedback. The lapse rate feedback (diamonds in Figs. 11–13) is strongly negative for both surface and atmospheric temperature. In an increased solar constant climate, the lapse rate decreases everywhere (Fig. 12b). First, the equatorial temperature increases, resulting in a lower moist-adiabatic lapse rate throughout the Tropics. Also, the amount of incoming solar radiation increases more in the Tropics than in high latitudes, resulting in an increased meridional temperature gradient. The increased meridional temperature gradient requires a lower lapse rate for baroclinic stability [see Eq. (3)]. Thus, the mid- and high-latitude lapse rate also decreases. Figure 12b shows that the lapse rate closely follows the atmospheric temperature regardless of which feedbacks (other than lapse rate) are disabled. Omitting the lapse rate increases the surface temperature change by about 70%. More complicated models (e.g., Wetherald and Manabe 1975; Hansen et al. 1984) have also produced a decreased lapse rate and negative lapse rate feedback in the Tropics for an increased solar constant. However, in high latitudes, these models produce a decreased meridional temperature gradient and an increased lapse rate. Our model differs because it does not include the surface albedo feedback (which amplifies high-latitude warming) and neglects the vertical distribution of radiative heating in the atmosphere.

A decreased lapse rate affects the effective longwave emission temperatures. The upward emission temperature increases, resulting in additional radiation to space, while the downward emission temperature decreases, resulting in less emission toward the ground. The net effect is a decrease in the greenhouse effect as the earth becomes more efficient at radiating to space. Thus, as the incoming solar radiation increases, the planet does not need to increase its temperature as much to balance incoming solar radiation with outgoing longwave radiation.

The lapse rate also has a strong effect on the emissivity of the atmosphere (Fig. 12a). As the atmospheric temperature increases, the lapse rate decreases, reducing the increase of the boundary layer temperature (Fig. 12c) and therefore resulting in a smaller emissivity change. When the lapse rate is not allowed to change (diamonds in Fig. 12), the emissivity is, therefore, higher in a warmer climate, further contributing to the greenhouse effect and warming the climate. Thus, the lapse rate feedback is negative on the emissivity in the sense that it reduces the strength of the emissivity feedback. This lapse rate–emissivity feedback, which reduces a positive temperature feedback, therefore has the same sign as the negative longwave radiation–lapse rate feedback, contributing to an overall negative lapse rate feedback on temperature.

The effect of the lapse rate feedback on boundary layer temperature is also seen in the response of the sensible heating to changes in atmospheric temperature (Fig. 13a). The effect of omitting the lapse rate feedback depends on the base climate state. For increases

(and small decreases) in the atmospheric temperature from the present value, the sensible heating decreases as the atmospheric temperature increases. However, for significant decreases in atmospheric temperature, the sensible heat decreases as the atmospheric temperature decreases. This reversal in the sensible heat change in the model without the lapse rate feedback is caused by the balance between two competing processes. First, with the lapse rate constant, the boundary layer temperature increases quickly with atmospheric temperature (Fig. 12c), contributing to a decrease in sensible heat. The surface temperature increases quickly with atmospheric temperature as well, suggesting an increase in sensible heat with atmospheric temperature. For low values of the atmospheric temperature, the dominant process is the surface temperature increase, while the boundary layer temperature effect becomes more important at higher atmospheric temperatures. Figure 13a illustrates the extreme sensitivity of the sensible heat to the model specifics. Because the sensible heat is proportional to the difference between two values that increase with the solar constant (boundary layer temperature and surface temperature), the specific magnitudes of these temperature changes are very important. For example, in an earlier version of the model with a different emissivity parameterization, we obtained a decrease of sensible heat everywhere for an increase in atmospheric temperature in the constant lapse rate case. The base model characteristics were essentially the same, and the behaviors of other variables as a function of atmospheric temperature were very similar. The behavior of sensible heating, though, was drastically different.

b. Meridional heat transport

Research suggests that meridional heat transport plays a significant role in the earth's climate sensitivity. Held and Suarez (1974) found that increasing the efficiency of poleward heat transport increases the sensitivity of an EBM with an ice–albedo feedback, assuming the same ice extent. They also suggest that the sensitivity could depend on the partitioning of transport between the ocean and atmosphere. Spelman and Manabe (1984), however, show that increasing ocean transport moves the ice extent poleward, reducing the climate sensitivity in a GCM.

More recently, researchers have studied the influence of an interactive ocean heat transport on climate sensitivity. Watterson (2003) obtains a slightly smaller climate sensitivity when comparing the Commonwealth Scientific and Industrial Research Organisation (CSIRO) Mark 2 coupled general circulation model with a mixed layer ocean version of the model. On the other hand, Stouffer and Manabe (1999) obtain a higher climate sensitivity in a coupled model compared to a mixed layer ocean version with prescribed heat transport, though they partially attribute it to a too-cool starting temperature. These results are also related to the effect heat transport has on the ice–albedo feedback.

Our model does not include the ice–albedo feedback. However, as a first step, we can test the response of the model to changes in the efficiency of meridional heat transport. In this case, we are not exploring the effect of transport on climate sensitivity to radiative forcing but, rather, we are examining the response of climate to transport itself. In this way, we can study the behavior of feedbacks within the system, specifically how they respond to changes in the meridional temperature gradient. These experiments do not have an exact analog for the earth's climate. The closest example might be changes in ocean transport efficiency related to different configurations of continents. However, we expect that some of the mechanisms that we find when the transport efficiency is changed would also modify the response to a climate forcing that changes the meridional temperature gradient.

To study the effect of meridional heat transport on the model, we varied the scale height parameter associated with the atmospheric eddy heat transport in Eq. (21). This parameter controls the effectiveness of eddies in decreasing the meridional temperature gradient. Changes in heat transport alone do not change the global average temperature because the transport merely rearranges the heat. Thus, any changes in the global average temperature must result from feedback processes that depend on the temperature gradient or on temperatures at a particular latitude.

As the eddy effectiveness is increased, the global average surface and atmospheric temperatures warm (Fig. 14). These increases are mostly caused by changes in the lapse rate. The decreased temperature gradient associated with more effective eddies results in an increased midlatitude lapse rate. In addition, the temperature in the Tropics decreases, increasing the moist-adiabatic lapse rate. The net effect is a global increase in lapse rate, resulting in an enhanced greenhouse effect through the reverse of the process described previously. When we exclude the lapse rate feedback (diamonds in Fig. 14), the effect of atmospheric heat transport on the global average temperature significantly decreases.

Another important feedback is the emissivity feedback, which amplifies the warmings. Although the increased transport decreases the temperature in the Tropics, resulting in a lower emissivity there, emissivity

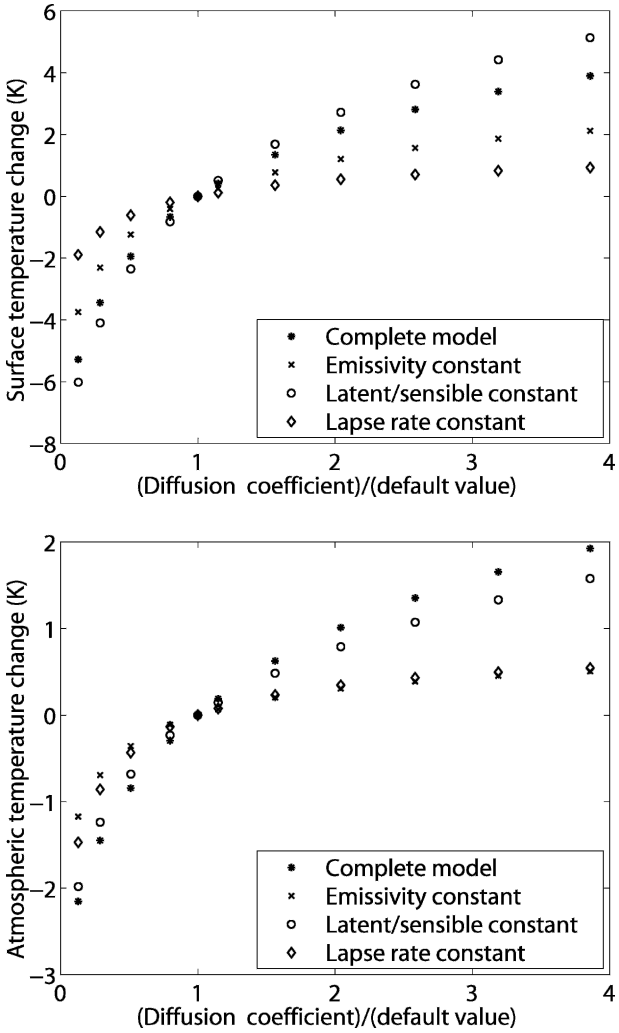

FIG. 14. Global average (top) surface and (bottom) atmospheric temperature change as a function of the atmospheric eddy transport efficiency. The temperature increases as the eddy efficiency increases, mostly as a result of the lapse rate feedback.

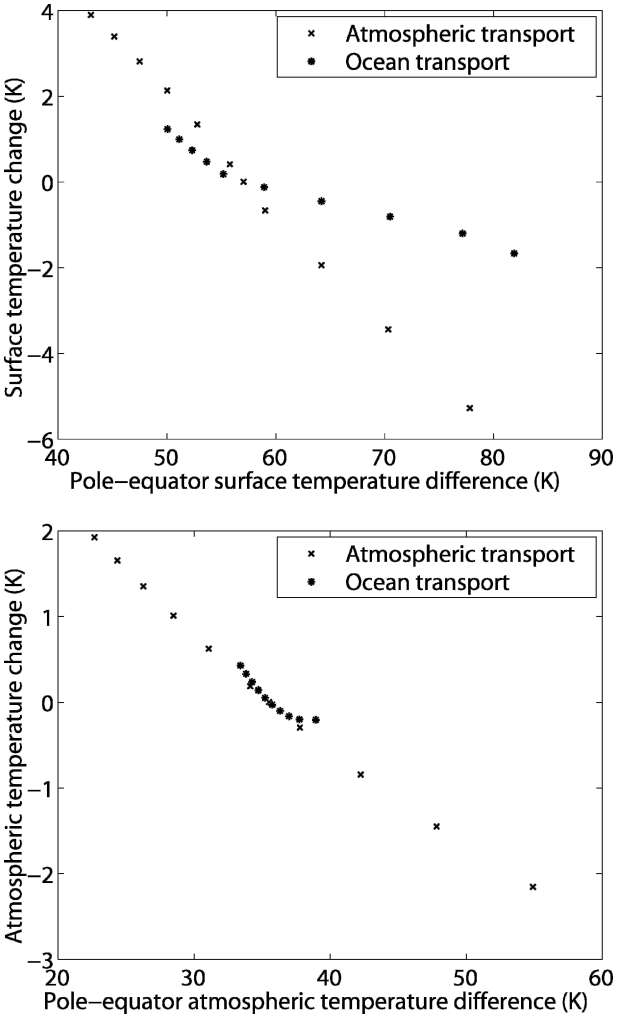

FIG. 15. Global average (top) surface and (bottom) atmospheric temperature change as a function of the pole-to-equator temperature gradient for different values of either the atmospheric or oceanic transport efficiency. Smaller temperature gradients correspond to warmer climates due to the lapse rate feedback.

changes are larger in the mid- and high latitudes, so the global average emissivity increases.

When latent and sensible heat feedbacks are excluded from the model, the surface temperature increases more than in the full model and the atmospheric temperature increases less. When the latent and sensible heat fluxes are allowed to vary, they increase as the diffusion effectiveness increases (increases in midlatitudes dominate decreases in the Tropics). Thus, the flux of heat from the surface to the atmosphere increases, slowing the warming of the surface and increasing the warming the atmosphere.

Figure 15 shows the global average temperature changes corresponding to different temperature gradients from the full model case described previously along with results from varying the ocean transport efficiency. Because the ocean transport is weaker than the atmospheric transport, we show temperature changes as a function of the resulting pole-to-equator temperature difference. An increase in the difference corresponds to a decrease in the efficiency of the transport. As the pole-to-equator temperature gradient increases, the climate cools. Thus, as meridional transport becomes more effective, the planet warms. Because the ocean transport has a stronger effect on the surface gradient than on the atmospheric gradient and the climate responds more to the atmospheric gradients, the surface temperature change is less for changes in ocean transport efficiency. However, the effect is of the same sign as the atmospheric eddy change effect.

5. Conclusions

We have developed a new climate model. Despite the simplicity of the model, it produces a reasonable present-day climate. The model captures much of the variation of temperature with latitude, and the global average energy balance is realistic. Given that the model excludes many details (e.g., the cloud and water vapor distribution related to the Hadley circulation) and considers only zonal and annual averages, the model's climate is more than adequate for its intended uses.

Though the model is based on the energy balance approach to modeling, it is distinctive in a number of ways. Rather than a single "column averaged" point at each latitude, our model explicitly calculates both a surface temperature and an atmospheric temperature. This separation allows for exploration of system behavior when the atmosphere and surface have different responses. Changes in latent and sensible heat fluxes, though they do not affect the TOA heat balance, can drastically affect the distribution of temperature response to different forcings, as shown in the solar constant sensitivity tests. Because our model treats the surface and atmosphere separately and thus explicitly determines heat fluxes between the two, not just as latent and sensible heat but also as radiative fluxes, the model is useful in studying processes that affect the surface and atmosphere differently.

Another distinction of the model is the use of a lapse rate that is dependent on climate. Although the model technically has only one atmospheric layer, this interactive lapse rate allows us to use different temperatures within the atmosphere for different processes. For example, the longwave emission by the atmosphere occurs at two different heights. The upper height corresponds to the effective blackbody radiating temperature of the atmosphere, as seen from space. The lower height corresponds to the effective temperature seen by the ground. These two heights are different because most longwave radiation does not pass through the atmosphere unabsorbed. The heights represent the location where upward or downward radiation is likely to reach space or the surface without being reabsorbed. The inclusion of an interactive lapse rate allows these effective temperatures to change as the structure of the atmosphere changes, as happens in the real atmosphere. In the model, as the planet warms, the lapse rate decreases, resulting in effective emission to space at a higher temperature and a negative feedback. We expect this feedback to be most realistic in the Tropics and midlatitudes. In high latitudes, the exclusion of the surface albedo feedback reduces the realism of the temperature change. Nevertheless, since our model includes an approximation of the lapse rate feedback, the model may be used to perform sensitivity studies in cases where simple models are needed (for computational or clarity reasons) and the lapse rate feedback is important.

While the model does not explicitly include any dynamical processes, we include parameterizations of the effects of atmospheric eddies, the Hadley circulation, and ocean circulation on the meridional transport of heat. We include these processes in more detail than is normally found in previous energy balance models. Because we specifically calculate a lapse rate, we are able to use the full Stone (1974) parameterization. (Most other simple models assume a constant lapse rate.) Thus, the transport of heat depends not only on the meridional temperature gradient but also on the vertical gradient, as baroclinic theory predicts. For the Hadley circulation, we adapted the Held and Hou (1980) assumption of angular momentum conservation to obtain a tropical atmospheric temperature profile subject to the conservation of energy. The net effect of this Hadley adjustment is that the Tropics tend to respond to forcings together as one unit, either all increasing or decreasing in temperature by the same amount. This corresponds approximately to our present understanding of the behavior of the Tropics, in that the tropical atmosphere is unable to maintain large temperature gradients. By testing the model sensitivity to changes in these meridional transport processes, we can see how the climate responds to different temperature gradients. For example, a larger pole-to-equator temperature gradient corresponds to a colder planet, while climates with smaller gradients are warmer.

Finally, an important aspect of this model is its simplicity. We are able to run multiple versions of the model quickly to explore feedbacks. The simplicity enables easy modification of the model, for example, to hold the latent and sensible heat fluxes constant to explore the effect on the atmosphere − surface temperature gradient. We can study the response of the climate to lapse rate changes by directly modifying the lapse rate. This task is much more difficult to accomplish in a GCM, where the combined effects of many different processes determine the change of temperature with height (or model level). Similarly, changes in the meridional temperature gradient are harder to isolate in GCMs. The speed and ease of use of our model are its greatest strengths.

To illustrate the benefits of this model, we perform a number of sensitivity studies. The sensitivity to solar constant changes is less than those obtained from other models, since our model does not include the ice–albedo feedback. In addition, the water vapor feedback

is too weak, and the lapse rate feedback is too strong. Thus, we cannot obtain an estimate of the total climate sensitivity with our model. However, we can use our model to estimate the sign and importance of specific feedbacks. In this paper, for example, we examine three feedbacks that affect the climate response to solar constant changes. The water vapor feedback enhances temperature changes. In addition, the feedback becomes stronger as the temperature decreases, resulting in nonlinearity of the temperature response. Our feedback is somewhat weaker than those obtained from other models, but given the limitations of the model's water vapor calculation, the resulting feedback is quite reasonable. The latent and sensible heat feedback affects the partitioning of warming between the surface and the atmosphere, almost halving the surface temperature response. Finally, the lapse rate feedback is strongly negative and serves to reduce the greenhouse effect. These feedbacks operate in conjunction with other feedbacks not studied (e.g., ice–albedo and cloud feedbacks) to determine the overall climate sensitivity.

Interactions among these different feedbacks can significantly alter the response. For example, sensible heat is determined by the difference between the boundary layer temperature and the surface temperature. Although both increase with the solar constant, the rates of increase are different. The net change in the sensible heat flux is very sensitive to feedbacks because they can alter the rates of increase, even changing the sign of the sensible heat change. Latent heating has a similar response to different feedbacks, but it is less severe since latent heat depends more closely on saturation specific humidity, which always increases with the solar constant. Another interaction is the effect the lapse rate has on the atmospheric emissivity, which further strengthens the negative lapse rate feedback.

We also examine the effect of meridional heat transport on the climate. As the effectiveness of atmospheric eddies increases, the temperature increases, mainly due to a global increase in the lapse rate. For the emissivity and latent and sensible heat changes, midlatitude increases outweigh tropical decreases as the eddy effectiveness increases, resulting in global average increases in these quantities. Thus, the emissivity feedback warms the planet, while the latent and sensible heat flux feedback reduces the warming of the surface.

While the model is already very fast, future work could focus on improving its computational efficiency, in addition to further exploration of climate feedbacks. Currently, the speed of the model is limited by the fact that the edge of the Hadley cell corresponds to a single grid point and thus can oscillate between grid points if the edge does not match the gridpoint location exactly. To solve this problem, we have increased the number of grid points and applied a damping to the atmospheric temperature change calculated by the Hadley parameterization. A better technique would be to allow the Hadley cell parameterization to linearly interpolate temperature between grid cells so that the edge does not have to correspond exactly to a grid point. Of course, this would complicate the Hadley cell parameterization, increasing the time required for a certain configuration. However, the model could be run at a lower resolution, resulting in an even faster model. Other Hadley cell adjustment methods could also be explored, which could further speed up the model. For example, one method would be to start with a particular southern critical latitude and integrate the temperature across the equator to the northern critical latitude, as determined from the equatorial temperature. Equation (24) is then minimized by trying different Southern Hemisphere critical latitudes and recalculating the integrals in Eq. (24). However, the model is already very fast, and we have not devoted extensive effort to improving computational efficiency.

Our model highlights some important interactions between different components of the climate system. However, when analyzing results, care should be taken to acknowledge the limitations of this model. Because all of the processes are highly simplified and many feedbacks, such as the ice–albedo feedback, are entirely eliminated, the absolute magnitudes of temperature responses to forcings are uncertain. Omitted processes may even change the sign of the response. However, the model provides an idea of which feedback processes might be important in the actual climate system and how certain feedbacks work when isolated from complications. Thus, our model, used with prudence, can be a useful tool for studying the climate system.

Acknowledgments. The authors wish to thank V. Ramanathan, Paola Cessi, Gerald North, and two anonymous reviewers for helpful insights and suggestions resulting in significant improvements to the manuscript. The authors also acknowledge the Data Assimilation Office at the Goddard Space Flight Center for producing the DAO data and Goddard's Distributed Active Archive Center for distributing the data. These activities are sponsored as part of NASA's Mission to Planet Earth program. The SRB and ERBE data were obtained from the NASA Langley Research Center Atmospheric Sciences Data Center.

This research was supported by NASA Headquarters under the Earth System Science Fellowship Grant NGT5-30446 and the Office of Science (BER), U.S. Department of Energy, Grant DE-FG02-97ER62338.

REFERENCES

Barkstorm, B., E. Harrison, G. Smith, R. Green, J. Kibler, R. Cess, and the ERBE Science Team, 1989: Earth Radiation Budget Experiment (ERBE) archival and April 1985 results. *Bull. Amer. Meteor. Soc.,* **70,** 1254–1262.

Budyko, M. I., 1969: The effect of solar radiation variations on the climate of the earth. *Tellus,* **21,** 611–619.

Claussen, M., and Coauthors, 2002: Earth system models of intermediate complexity: Closing the gap in the spectrum of climate system models. *Climate Dyn.,* **18,** 579–586.

Eady, E. T., 1949: Long waves and cyclone waves. *Tellus,* **1,** 33–52.

Grist, J. P., and S. A. Josey, 2003: Inverse analysis of the SOC air–sea flux climatology using ocean heat transport constraints. *J. Climate,* **16,** 3274–3295.

Gupta, S. K., N. A. Ritchey, A. C. Wilber, C. H. Whitlock, G. G. Gibson, and N. A. Ritchey, 1999: A climatology of surface radiation budget derived from satellite data. *J. Climate,* **12,** 2691–2710.

Hansen, J., A. Lacis, D. Rind, G. Russell, P. Stone, I. Fung, R. Ruedy, and J. Lerner, 1984: Climate sensitivity: Analysis of feedback mechanisms. *Climate Processes and Climate Sensitivity,* J. E. Hansen and T. Takahashi, Eds., Amer. Geophys. Union, 130–163.

Held, I. M., and M. J. Suarez, 1974: Simple albedo feedback models of the icecaps. *Tellus,* **26,** 613–629.

——, and A. Y. Hou, 1980: Nonlinear axially symmetric circulations in a nearly inviscid atmosphere. *J. Atmos. Sci.,* **37,** 515–533.

Houghton, J. T., Y. Ding, D. J. Griggs, M. Noguer, P. J. van der Linden, X. Dai, K. Maskell, and C. A. Johnson, Eds., 2001, *Climate Change 2001: The Scientific Basis.* Cambridge University Press, 881 pp.

Kiehl, J. T., and K. E. Trenberth, 1997: Earth's annual global mean energy budget. *Bull. Amer. Meteor. Soc.,* **78,** 197–208.

Liou, K. N., 2002: *An Introduction to Atmospheric Radiation.* 2d ed. Academic Press, 583 pp.

Manabe, S., and R. T. Wetherald, 1967: Thermal equilibrium of the atmosphere with a given distribution of relative humidity. *J. Atmos. Sci.,* **24,** 214–259.

North, G. R., R. F. Cahalan, J. James, and A. Coakley, 1981: Energy balance climate models. *Rev. Geophys. Space Phys.,* **19,** 91–121.

Pujol, T., and G. R. North, 2002: Runaway greenhouse effect in a semigray radiative–convective model. *J. Atmos. Sci.,* **59,** 2801–2810.

Ramanathan, V., 1977: Interactions between ice-albedo, lapse-rate and cloud-top feedbacks: An analysis of the nonlinear response of a GCM climate model. *J. Atmos. Sci.,* **34,** 1885–1897.

——, 1981: The role of ocean–atmosphere interactions in the CO_2 climate problem. *J. Atmos. Sci.,* **38,** 918–930.

Schubert, S. D., J. Pjaendtner, and R. Rood, 1993: An assimilated dataset for earth science applications. *Bull. Amer. Meteor. Soc.,* **74,** 2331–2342.

Sellers, W. D., 1969: A global climatic model based on the energy balance of the earth-atmosphere system. *J. Appl. Meteor.,* **8,** 392–400.

Spelman, M. J., and S. Manabe, 1984: Influence of oceanic heat transport upon the sensitivity of a model climate. *J. Geophys. Res.,* **89,** 571–586.

Staley, D. O., and G. M. Jurica, 1972: Effective atmospheric emissivity under clear skies. *J. Appl. Meteor.,* **11,** 349–356.

Stone, P. H., 1974: The meridional variation of the eddy heat fluxes by baroclinic waves and their parameterization. *J. Atmos. Sci.,* **31,** 444–456.

——, 1978: Baroclinic adjustment. *J. Atmos. Sci.,* **35,** 561–571.

Stouffer, R. J., and S. Manabe, 1999: Response of a coupled ocean–atmosphere model to increasing atmospheric carbon dioxide: Sensitivity to the rate of increase. *J. Climate,* **12,** 2224–2237.

Thompson, S., and D. Pollard, 1997: Greenland and Antarctic mass balances for present and doubled CO_2 from the GENESIS version-2 global climate model. *J. Climate,* **10,** 871–900.

Trenberth, K. E., and J. M. Caron, 2001: Estimates of meridional atmosphere and ocean heat transports. *J. Climate,* **14,** 3433–3443.

Watterson, I. G., 2003: Effects of a dynamic ocean on simulated climate sensitivity to greenhouse gases. *Climate Dyn.,* **21,** doi:10.1007/s00382-003-0326-4.

Wetherald, R. T., and S. Manabe, 1975: The effects of changing the solar constant on the climate of a general circulation model. *J. Atmos. Sci.,* **32,** 2044–2059.